J. Meas. Sci. Instrum., 2024, 15(4): 432-444.
DOI: 10.62756/jmsi.1674-8042.2024044
http://jmsi.publish.founderss.cn
jmsi@nuc.edu.cn

The lift-off effect analysis of flexible differential pick-up koch fractal eddy current probe

CHEN Guolong*, FAN Le, ZHANG Shuaishuai, HAN Yu, LI Yixin, ZHANG Yanlong
School of mechanical and electrical engineering, Lanzhou university of technology, Lanzhou 730050, China

***Corresponding author:** CHEN Guolong (guolongchen@lut.edu.cn)

Received: June 1, 2024 **Revised:** August 4, 2024 **Accepted:** September 2, 2024

Abstract: This study utilized finite element simulation and experimental methods to investigate the evolution of crack detection performance of a flexible differential fractal Koch eddy current probe at different excitation frequencies as the lift-off distance increases. As the lift-off distance increased, the distribution shape of induced eddy currents changed, leading to reduced similarity in the shape of the excitation coil and an expanded distribution range of induced eddy currents, ultimately resulting in weakened output signal strength. The experimental results showed that for excitation frequencies of 10 kHz, 20 kHz, 50 kHz, 100 kHz, 200 kHz, 500 kHz, and1 000 kHz, the maximum lift distances of the real part of the output signal when cracks were detected were 5.0 mm, 7.0 mm, 8.0 mm, 8.0 mm, 8.0 mm, 6.5 mm, and 4.0 mm, respectively. The imaginary parts were 6.5 mm, 6.5 mm, 7.5 mm, 5.5 mm, 8.0 mm, 6.5 mm, and 6.5 mm, respectively.
Key words: eddy current testing; lift-off effect; nondestructive testing; crack detection; fractal geometry

0 Introduction

Eddy current testing (ECT) is widely used for non-destructive testing and structural integrity evaluation of metallic components due to its benefits, such as non-contact operation, rapidity, and efficiency[1]. The eddy current (EC) probe is the starting point of the ECT system for obtaining information, and its performance directly affects the quality of the inspection results[2]. With changes in function, load-bearing capacity, and service conditions, the morphology of metallic components is becoming increasingly complex. This complexity results in disadvantages for traditional three-dimensional rigid probes, such as more difficult-to-detect areas and susceptibility to lift-off (LF) noise. Therefore, flexible EC probes that can be customized to the morphology of the object under test have been proposed. Examples include the internal differential multichannel flexible probe for curved microcrack detection, and the flexible probe for detecting carbon fiber reinforces polymers[3-5].

In the process of ECT, the change in output signal caused by variations in LF distance is called the LF effect[6]. Installation errors, non-horizontal inspection surfaces, corrosion-resistant coatings, and part wrapping inevitably lead to changes in LF distance, affecting detection results. Therefore, the crack detection performance of EC probes are studied when LF distance varies is necessary for their operation under large and variable LF distances. For example, in defect detection of the U-shaped alternating current field measurement (ACFM) system, Li et al.[7] used the linear least squares fitting method to examine the relationship between LF distance and electromagnetic signal amplitude, determining that the optimal LF distance for defect detection was 4 mm through simulation and experimentation. In the electromagnetic ultrasonic detection system, Huang et al.[8] analyzed the distribution and strength of the alternating magnetic field at different LF distances by simulation and experiment. To study the LF effect of the EC probe under multi-frequency excitation, Marco Ricci et al.[9] examined the impact of LF distance variation on amplitude and phase imaging. The results indicate that phase analysis yields more robust images, whereas amplitude analysis is more susceptible to LF distance changes.

The signal compensation method suppresses the LF effect by post-processing the signal. While this method requires complex algorithms, innovations in probe structure design can suppress the LF effect at the onset of information acquisition[10,11]. For example, changes to the coil shape, excitation method, and coil spatial layout

can be implemented. Chen et al.[12] proposed a two-layer differential planar coil, where the upper layer consisted of two symmetrical excitation coils that produced symmetrical and reversely amplified magnetic fields. The lower layer features a rectangular detection coil with a differential structure, allowing the probe to identify individual microcracks at an LF distance of 3 mm. Hoshi Kawa et al.[13] developed a probe that generated uniform eddy currents, inducing a uniformly distributed EC in the measured material. Its self-zeroing characteristic effectively eliminates most LF noise. Huang et al.[14] introduced a new four-coil probe structure that aimed at eliminating the impact of LF noise on the detection signal, thereby improving the signal-to-noise ratio. Liu et al.[15] proposed a differential probe designed to suppress the LF effect in pulsed EC detection.

To further study the mechanism of the LF effect and the evolution of the eddy currents caused by the excitation coil at different LF distances, Chen et al.[16] proposed two indices based on information entropy to evaluate the similarity between the EC distribution and the shape of the excitation coil, as well as the concentration of the EC distribution in relation to variations in LF distance. The results indicate that as LF distance increases, the similarity between the shapes of the EC distribution and the excitation coil tends to decrease, accompanied by a dispersion in the concentration of the EC distribution. Subsequently, Chen et al.[17] introduced relative entropy and cross-entropy to evaluate the differences between the EC distributions of the Koch and circular coils as LF distance changes. However, the crack detection performance of the fractal EC probe under varying LF distances has yet to be studied.

A flexible differential pick-up Koch fractal EC probe was proposed based on the probe structure design. The probe coil was manufactured on a flexible printed circuit (FPC), allowing it to bend and adapt to the complex shapes of metal components for crack detection. A multi-turn winding differential signal pick-up coil enhances detection signal strength while simultaneously avoiding the LF effect, enabling non-destructive detection under both large and variable LF conditions. In this study, the evolution of the probe's crack detection performance with increasing LF distance at different excitation frequencies was investigated. The maximum LF distance at which the probe could detect cracks for each excitation frequency was examined through both simulation and experiment.

1 Probe design

1.1 Coil structure

The flexible differential pick-up Koch fractal EC probe operates in transmit-receive mode and consists of two parts: the excitation coil and the pick-up coil. The excitation coil is a single-turn third-order Koch curve[18]. It has a diameter of 10 mm and a line width of 0.05 mm, as shown in Fig. 1(a). This probe adopts a third-order Koch curve for its coil structure because, compared to lower-order curves, the third-order Koch curve has a more complex geometric design. Notably, in the triangular sections formed at the outer circle position of the Koch curve, significant eddy current disturbances are generated. Additionally, the unique geometric structure of the Koch curve can adjust the eddy current vector in multiple directions locally, increasing the probability of disturbances caused by cracks in various orientations, thereby improving the probe's detection rate for cracks.

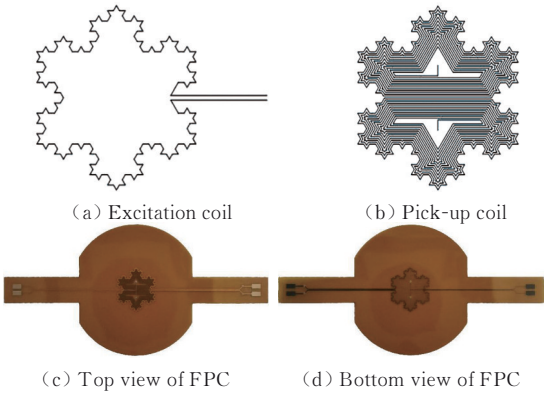

Fig. 1 Structure of probe

The pick-up coil consists of 12 turns, with the two coils reversed at the midpoint, maintaining a distance of 0.05 mm between adjacent turns and a wire width of 0.05 mm, as shown in Fig. 1(b). The reversed winding of the pick-up coil enables differential detection. Both the excitation and pick-up coils are fabricated on a four-layer FPC. The top layer is padded, as shown in Fig. 1(c). The exciting coil is located in the third layer, and the picking coil is located in the second layer. The bottom layer serves as the protective layer, as shown in Fig. 1(d). The completed flexible probe is secured at the bottom of the pre-designed housing, with the terminals of both coils connected to an SMA connector via wires to link to the experimental system.

1.2 Working principle

To establish the equivalent circuit model of the probe in the crack detection process, the equivalent transimpedance

expression that characterizes the probe's output signal is determined. An analysis is conducted on the factors affecting the probe's performance in crack detection, as well as those influenced by changes in the LF distance. Initially, the equivalent inductance of the pick-up coil is determined using mutual inductance equivalent decoupling, leading to the construction of a decoupling model for the pick-up coil. Subsequently, the equivalent circuit model of the probe is established, and the expression for the equivalent transimpedance of the probe is derived. The output signal of the probe is characterized by this equivalent transimpedance.

The pick-up coil of the probe can be represented as a series connection of two coils and a resistor, with its equivalent circuit shown in Fig. 2(a). The mutual inductance equivalent decoupling model of the pick-up coil is shown in Fig.2(b). L_{2L} and L_{2R} represent the equivalent inductance of the two pick-up coils based on the differential structure, while R_2 is the equivalent resistance of the pick-up coil, m is the mutual inductance between the two coils, and V and I are the voltage added to both ends of the circuit and the current in the circuit, respectively. According to Kirchhoff's voltage law, there is

$$V=\left(\mathrm{j}\omega L_{2L}+\mathrm{j}\omega L_{2R}+2\mathrm{j}\omega+R_2\right)I. \tag{1}$$

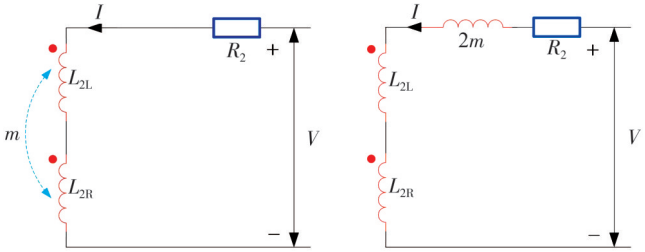

(a) Before decoupling (b) After decoupling

Fig. 2 Equivalent circuit of pick-up coil

After equivalent decoupling, the inductance of the pick-up coil can be equated to

$$L_{equ}=L_{2L}+L_{2R}+2m. \tag{2}$$

The equivalent circuit model of the probe for detecting cracks is shown in Fig. 3. V_S is the excitation voltage. V_0 is the output voltage of the probe. R_1 is the equivalent resistance of the excitation coil. L_1 is the equivalent inductance of the excitation coil. R_S is the internal resistance of the excitation module. R_3 and L_3 are the equivalent resistance and inductance of the specimen, respectively. R_{load} is the input impedance of the signal conditioning circuit. I_1 is the excitation current. I_2 is the current in the pick-up coil. I_3 is the equivalent induced current in the specimen. M_{12L} and M_{12R} are the mutual inductance between the excitation and the two pick-up coils of the differential structure. M_{13} is the mutual inductance between the excitation coil and the specimen. M_{32L} and M_{32R} are the mutual inductance between the specimen and the two parts of the pick-up coil. According to Kirchhoff's voltage law, there are

$$\begin{cases} V_S=I_1(R_S+R_1+\mathrm{j}\omega L_1)+I_3\mathrm{j}\omega M_{13}+I_2\mathrm{j}\omega \\ \qquad (M_{12L}-M_{12R}), \\ V_0=I_2(R_2+2\mathrm{j}\omega m+\mathrm{j}\omega L_{2L}+\mathrm{j}\omega L_{2R})+I_1\mathrm{j}\omega \\ \qquad (M_{12L}-M_{12R})+I_3\mathrm{j}\omega(M_{32L}-M_{32R}), \\ I_3R_3+I_3\mathrm{j}\omega L_3+I_1\mathrm{j}\omega M_{13}+I_2\mathrm{j}\omega(M_{32L}-M_{32R})=0. \end{cases} \tag{3}$$

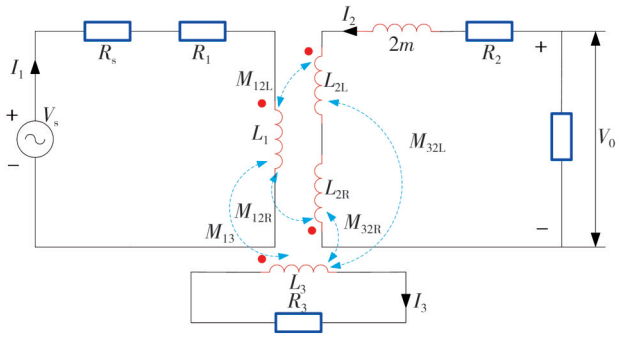

Fig. 3 Equivalent circuit of probe

Since the input impedance of the preamplifier is at the GΩ level, to simplify the analysis, it is assumed to be infinite, i.e., $R_{load}=\infty$, so $I_2=0$. And $M_{12L}=M_{12R}$, so Eq. (3) can be simplified as

$$\begin{cases} V_S=I_1(R_S+R_1+\mathrm{j}\omega L_1)+I_3\mathrm{j}\omega M_{13}, \\ V_0=I_3\mathrm{j}\omega(M_{32L}-M_{32R}), \\ I_3R_3+I_3\mathrm{j}\omega L_3+I_1\mathrm{j}\omega M_{13}=0. \end{cases} \tag{4}$$

The equivalent trans-impedance of the probe is

$$Z_{req}=\frac{\omega^2M_{13}(M_{32L}-M_{32R})}{R_3{}^2-\omega^2L_3{}^2}R_3-\mathrm{j}\frac{\omega^3M_{13}(M_{32L}-M_{32R})}{R_3{}^2-\omega^2L_3{}^2}L_3. \tag{5}$$

The factors affecting the equivalent trans-impedance of the probe include ω, M_{13}, M_{32L}, M_{32R}, R_3, and L_3. Under the condition of constant ω, when the morphology of the specimen or the crack changes, it will cause the change of R_3 and L_3, resulting in the change of equivalent trans-impedance. When the LF distance changes, M_{13}, M_{32L}, and M_{32R}, R_3, and L_3 all change, thus affecting the crack detection performance of the probe.

The equivalent trans-impedance is used as the output signal of the probe. When the probe is placed in parallel above the crack-free specimen, $M_{32L}=M_{32R}$, obtained from Eq. (5), $Z_{req}=0$, the output signal of the probe is zero to achieve the effect of self-nulling. When there is a crack in the specimen, due to the crack on the induction EC disturbance, which changes the original path of the EC. When there is a crack in the specimen, the original path of

the EC is changed due to the disturbance of the crack, and the crack causes the mutual inductance between the specimen and the two pick-up coils to be unequal, i.e., $M_{32L} \neq M_{32R}$, so $Z_{req} \neq 0$, and the signal is not zero.

The working principle of the probe is shown in Fig.4. An alternating exciting current I_1 is passed into the excitation coil, and a changing spatial primary magnetic field is generated. When the magnetic field on the inside of the excitation coil is directed upward, this magnetic field acts on the specimen part, EC is generated in the conductive specimen, and a secondary magnetic field is generated simultaneously. The distribution of the primary and secondary magnetic fields is similar but in opposite directions, and through the mutual inductance M_{12L}, M_{12R}, M_{32L}, and M_{32R}, the pick-up coil generates induced voltages[12].

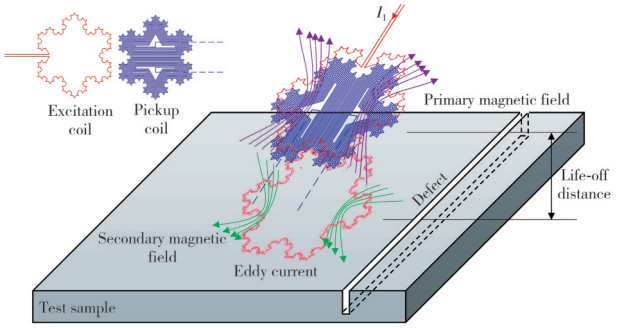

Fig. 4 Principle of differential pick-up probe

When the probe detects cracks in the specimen, the presence of a crack alters the equivalent resistance and inductance of the specimen. Additionally, the relative position between the crack and the two pick-up coils varies, leading to different degrees of mutual induction between the specimen and each coil. Consequently, $M_{32L} \neq M_{32R}$, resulting in a non-zero output signal from the probe. During actual crack detection, various test conditions and errors related to the processing and installation of the probe may introduce background noise, causing the signal to deviate from zero. When the probe identifies a crack, the disturbance caused by the crack affects the electromagnetic characteristics on the specimen's surface. This crack signal rises above the background noise, exhibiting distinct features such as characteristic wave crests and troughs. These unique signals are utilized to confirm the presence of the crack.

2 Finite element analysis

In order to study the LF effect, the EC distribution induced by the probes, and the crack detection performance, finite element (FE) analysis of the detection process of the probe was performed with the software COMSOL Multiphysics. Firstly, finite element analysis was performed on the model of the probe above the specimen, studying the effect of variation of LF distance on the EC distribution on the specimen's surface. Then, the finite element analysis was carried out to study the influence of LF distance change on the crack detection results under different excitation frequency.

2.1 Finite element model

The geometric model comprised an air domain, a specimen, and structure coils, with the coil structure positioned above thealuminum specimen at a specified LF distance. The specimen included two types in the model: specimens with cracks and specimens without cracks. Fig. 5(a) illustrates the geometric setup for detecting specimens without cracks, while Fig.5(b) shows the model used for detecting specimens with cracks, where the crack dimensions are 35 mm in length, 0.25 mm in width, and 3 mm in depth. Additional physical parameters of the air domain and specimen can be found in Table 1. A side current of 1 A is applied to the excitation coil. The geometric model is finely meshed using physics-controlled grids for finite element analysis.

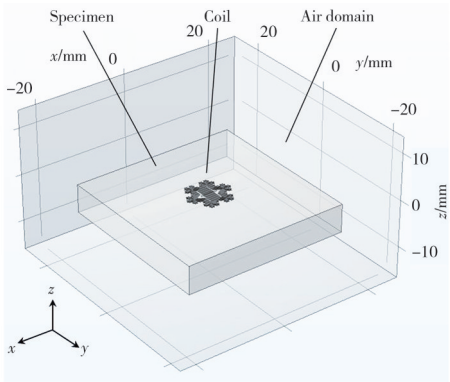

(a) Without a crack

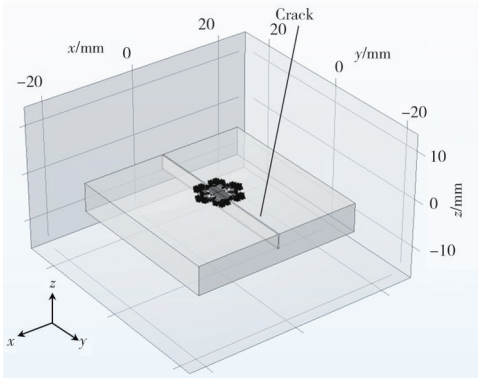

(b) With a crack

Fig. 5 Geometric model

In the FE analysis, the EC distribution on the surface of the specimen and the crack signal is investigated at excitation frequencies of 10 kHz, 20 kHz, 50 kHz,

100 kHz, 200 kHz, 500 kHz, and 1 000 kHz, with LF distance of 0.1 mm, 0.5 mm, 1.0 mm—8.0 mm (with the step of 1.0 mm), respectively. In the finite element models (FEMs), the excitation and pick-up coil positions were kept constant still, and the crack movement was used to simulate the scanning process of the probe[19].

Table 1 Physical parameters of FEMs

Parameter	Size/ mm×mm×mm	Relative permeability	Relative permittivity	Electrical conductivity/ $S \cdot m^{-1}$
Air	50×50×30	1	1	10
Specimen	35×35×6	1	1	3.774×10^7

2.2 Finite element analysis results

2.2.1 Effect of LF distance on distribution of induced EC

Fig. 6 shows the EC distribution on the surface of the specimen when the excitation frequency is 10 kHz. It can be seen that when the LF distance is 0.1 mm, the distribution of EC on the specimen's surface is similar to the shape of the excitation coil, and the EC density is strongest directly below the excitation coil. With the increase of LF distance, the EC distribution area starts to disperse in all and eventually evolves into a circle.

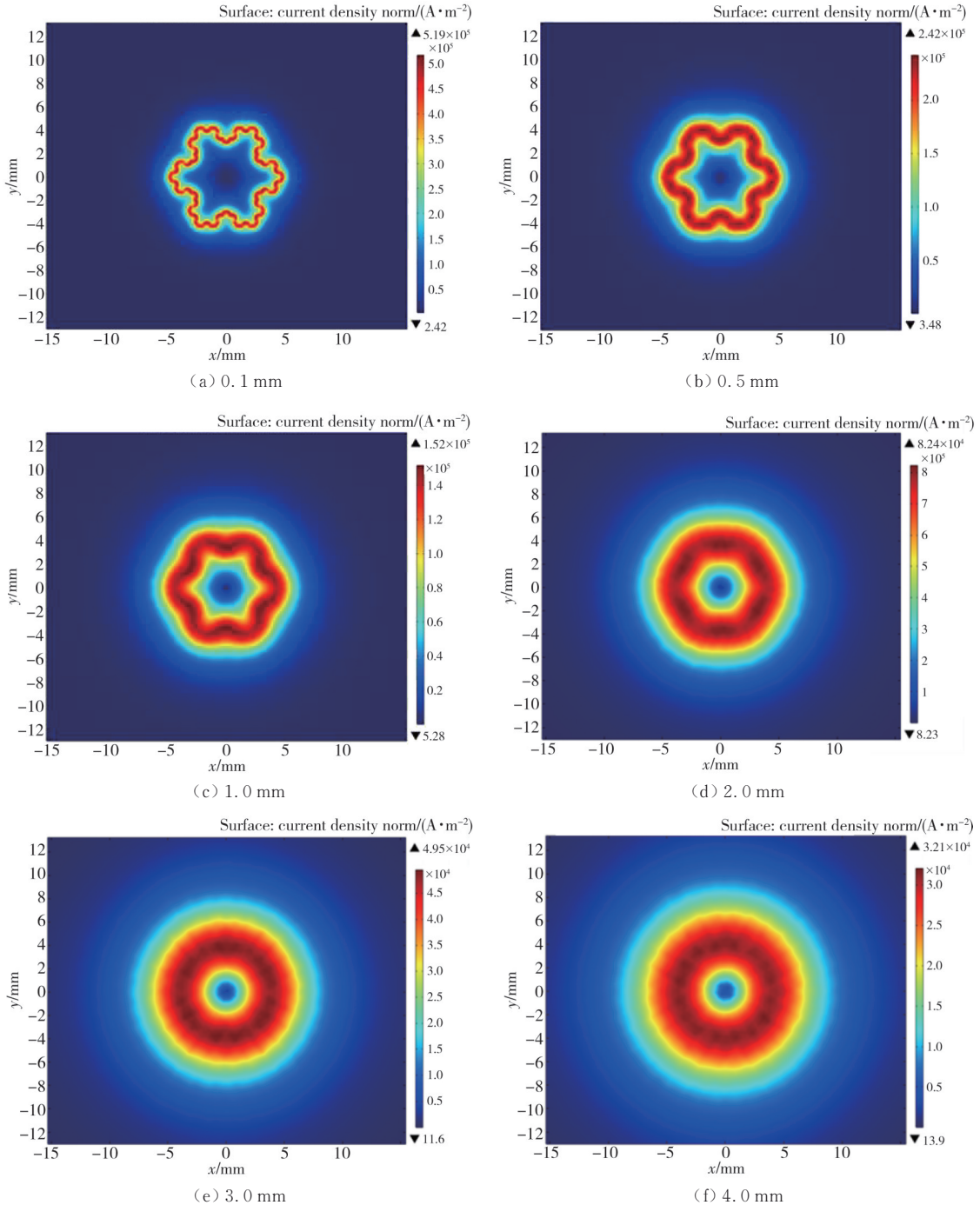

(a) 0.1 mm (b) 0.5 mm

(c) 1.0 mm (d) 2.0 mm

(e) 3.0 mm (f) 4.0 mm

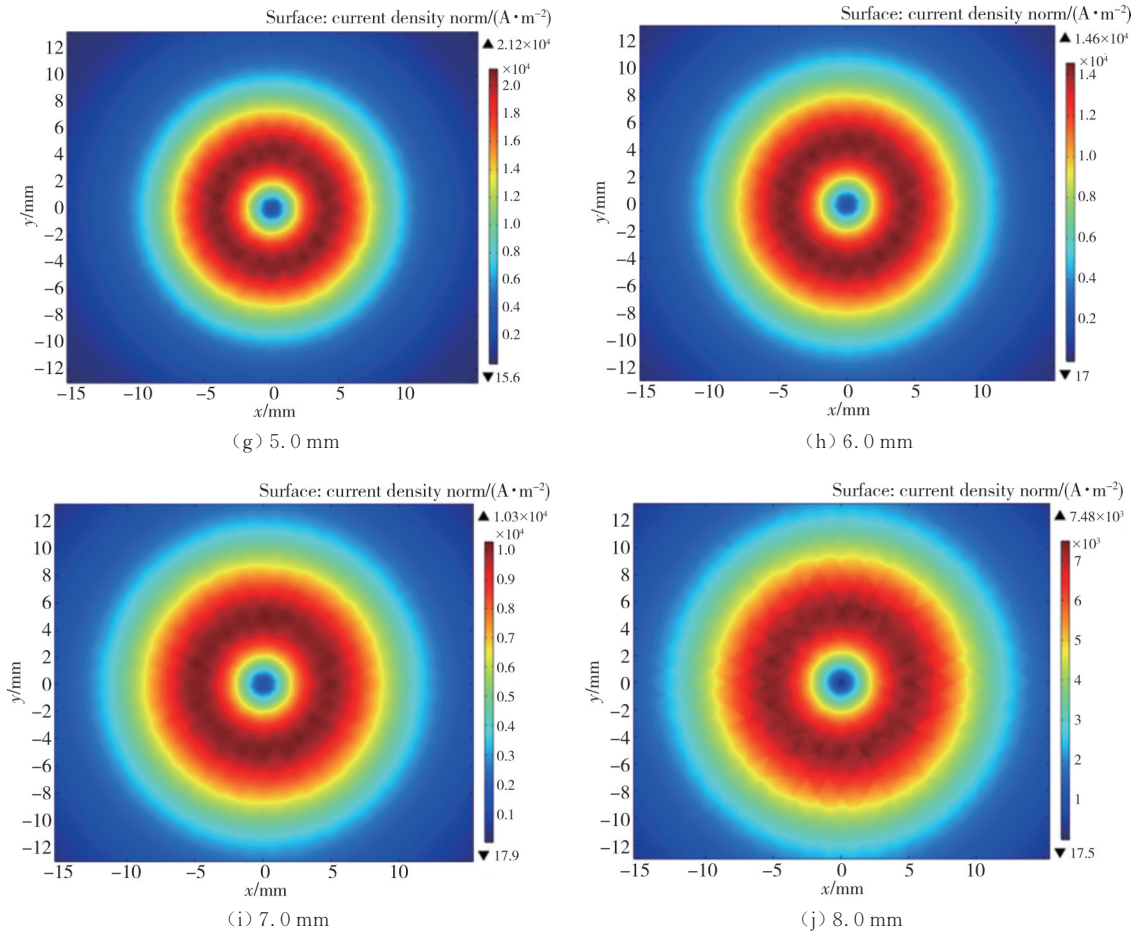

Fig. 6 EC distributions on specimen's surface

The higher the LF distance, the wider the area of EC distribution. This phenomenon is similar to the results in the Ref.[16]. The increase in the LF distance causes an increase in the distribution area of the EC, but leads to a weakening of the intensity of the EC simultaneously, which reduces the chance of cracking and EC interaction.

Fig.7 illustrates the trend of the maximum value of the electric field induced by the probe on the surface of the specimen as a function of LF distance at different excitation frequencies. Under the same excitation frequency, the maximum value of EC density decreases exponentially with increasing LF distance. At a constant LF distance, a higher excitation frequency results in a greater maximum value of EC induced on the specimen's surface. This occurs because a higher excitation frequency causes more significant changes in the primary magnetic field generated by the same excitation current, leading to stronger electromagnetic induction within the specimen and, consequently, a more pronounced EC distribution on its surface. As the LF distance increases, the primary magnetic field reaching the specimen's surface weakens, resulting in reduced electromagnetic induction and lower EC density.

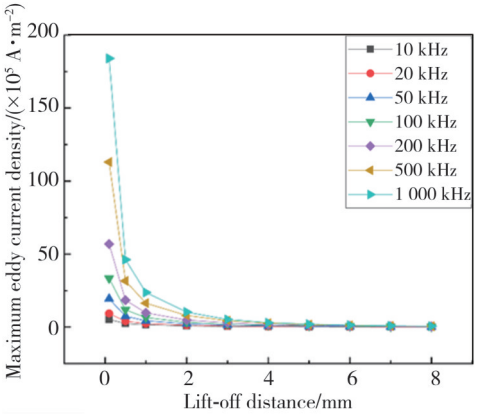

Fig. 7 Variation of maximum induced eddy current density on specimen's surface with LF distance under different excitation frequencies

2.2.2 Effect of LF distance on crack signal

When the LF distance increases to 4.5 mm, the real part of the signal is drowned out by the background noise, and it is impossible to evaluate whether the crack exists or not. However, the imaginary part of the signal still shows the crack characteristics, and the signal change appears when the crack exists. Fig.8(b) shows the imaginary part of the signal. As the LF distance increases until it reaches 8.0 mm, the crack information

is still present in the imaginary part of the signal. At a LF distance of 0.1 mm, both the real and imaginary parts of the signals exhibit characteristics of sinusoidal waves. However, as the LF distance increases to 4.5 mm and 8 mm, the real part of the output signal becomes submerged in noise, while the imaginary part shows a phase reversal in the sinusoidal waveform.

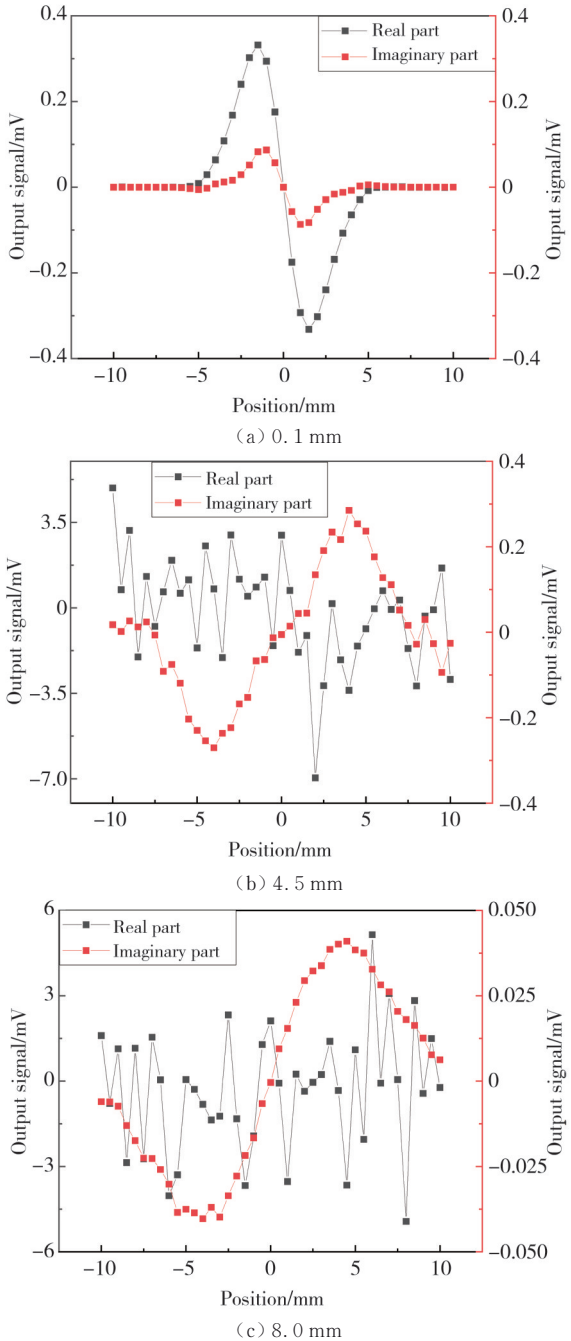

Fig. 8 Output signal of probe at different LF distances

As the probe moves further away from the increasing LF distance, the amplitude of the eddy current signal decreases due to attenuation. This reduction in signal strength relative to noise levels can cause the real part of the signal to become less distinguishable, eventually being overshadowed by noise. Fig.8(c) is the imaginary part signal at the LF distance. The Vpp of the imaginary parts of the signal are 1.73×10^{-4} V, 5.55×10^{-7} V, and 8.13×10^{-8} V at the LF distance of 0.1 mm, 4.5 mm, and 8.0 mm, respectively, and the Vpp are reduced by four orders of magnitude.

Fig. 9 shows the Vpp of the signals at different LF distances. The real and imaginary Vpp of the output signal decreases with the increase of the LF distance, and the Vpp changes less and less when the LF increases to a certain distance.

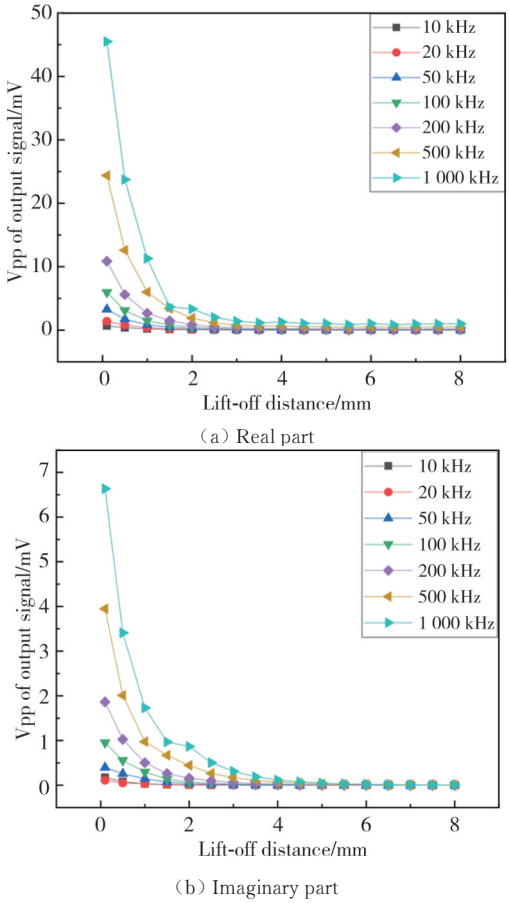

Fig. 9 Vpp of probe for different LF distances at each excitation frequency

The Vpp increases with the increase of the excitation frequency. This is because as the LF distance increases, the primary magnetic field generated on the surface of the specimen decreases. It weakens the EC on the specimen surface, and the disturbance between EC and the crack is weakened at this time, resulting in a decrease in Vpp. A 10 kHz excitation frequency was taken as an example. When the LF distance is greater than or equal to 4.5 mm, the Vpp tends to be zero. Therefore, the Vpp of the real part is inaccurate and has no reference significance after 4.5 mm LF distance. As the LF distance increases, there is a corresponding decrease in the signal-to-noise ratio.

When the LF distance reaches a certain point, the intensity of the background noise surpasses that of the detection signal, completely obscuring useful information. At this stage, it becomes impossible to determine whether a crack is present.

3 Experiment

3.1 Experimental system

To investigate the LF effect and the crack detection performance of the probe, as well as to determine the maximum LF distance at which cracks can be detected for each excitation frequency, an experimental system similar to the Ref.[20] was constructed. The probe was mounted on a 3D scanner, and a sinusoidal signal was generated by the RIGOL-DG832 signal generator, which was then amplified by the RIGOL-PA1011 power amplifier. The effective value of the excitation current was continuously monitored using a RIGOL-DM3058 digital multimeter, and the excitation current was ultimately fed into the excitation coil. The voltage signal detected by the pick-up coil was amplified 200 times by an AIGTEK-ATA-5210 pre-amplifier. This signal was then processed by an OE2031 lock-in amplifier, which combined the detected signal with a reference signal generated by the signal generator. The processed data was extracted to a computer via software for easy viewing and further analysis. The schematic and physical diagrams of the experimental system are shown in Figs. 10 and 11.

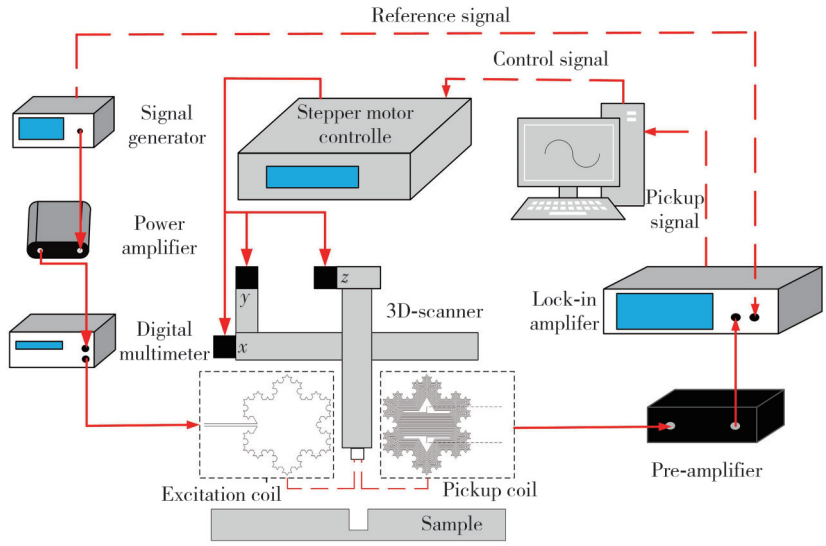

Fig. 10 Schematic diagram of experimental system

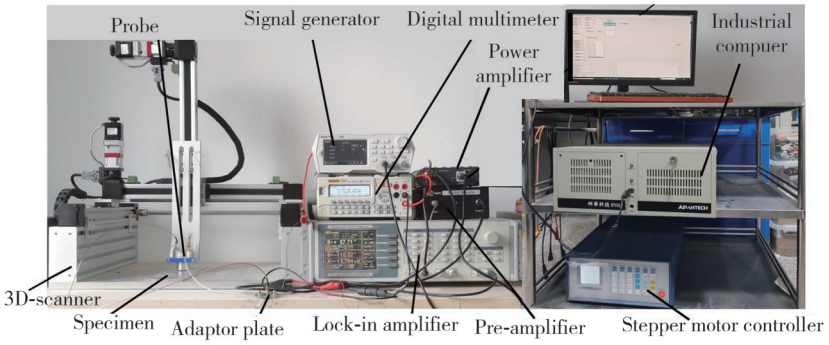

Fig. 11 Photograph of experimental system

Fig.12 shows a photograph of the aluminum specimen used in this experiment. The specimen is aluminum, with dimensions of 350 mm×80 mm×6 mm. A prefabricated crack measuring 80 mm×0.25 mm×3 mm is etched onto the aluminum specimen. The movement of the probe is controlled by a stepper motor controller, with control signals transmitted via serial communication and issued by upper-level software programmed in C#. During the scanning process, the stepper motor controller sends 224 advance signals to the stepper motor, causing the probe to move forward by 0.24 mm.

MATLAB was used for the obtained output signal to detrend it and find the Vpp corresponding to each waveform plot. In this work, the probe equivalent trans-

impedance Z is used as the signal, which is calculated by

$$Z=\frac{V_{\mathrm{p}}}{kI_e}=Real\left(\frac{V_{\mathrm{p}}}{kI_{\mathrm{e}}}\right)+\mathrm{j}Imaginary\left(\frac{V_{\mathrm{p}}}{kI_{\mathrm{e}}}\right), \quad (6)$$

where V_{P} denotes the induced electric potential difference detected by the pick-up coil; I_{e} denotes the amplitude of the excitating current, and k denotes the amplification of the pre-amplifie based on the above experimental system. The experiments were performed at different LF distances and excitating frequencies were same to the FEMs.

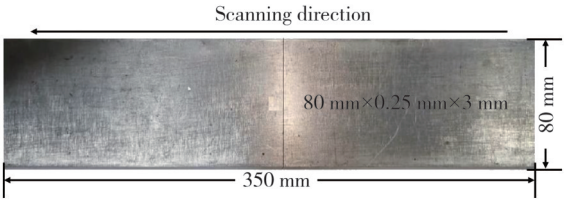

Fig. 12 Specimen of photograph

3.2 Experimental results

Fig. 13 shows the output signals of the probe at different LF distances when the excitation frequency is set to 10 kHz. As the LF distance increases, the intensity of the crack signal detected by the probe decreases, while the interference from LF noise to the detection signal increases. The difference between the output signal and that at a 0.1 mm LF distance grows larger, with the output signal approaching zero. This reduction is due to the increased LF distance, which weakens the induction EC density on the specimen's surface and diminishes the interaction between the crack and the induction EC. The ability of the probe to continue detecting cracks becomes increasingly dependent on factors such as the probe's design structure, coil shape, processing accuracy, and other variables. The maximum LF distance at which the real part of the signal can detect the crack is 5.0 mm, as shown in Fig. 14(a), while the maximum LF distance for the imaginary output signal detection is 6.5 mm, illustrated in Fig.14(b).

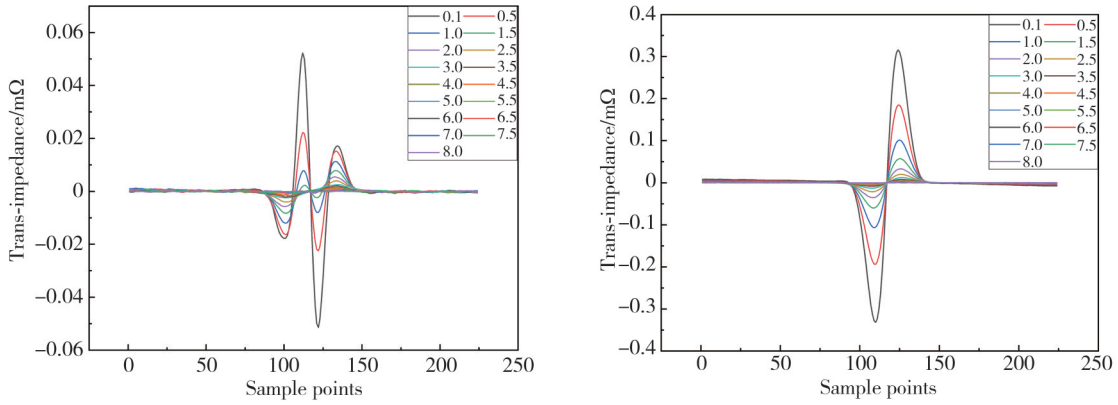

(a) Real part (b) Imaginary part

Fig. 13 Probe output signals at different LF distances at 10 kHz excitation frequency

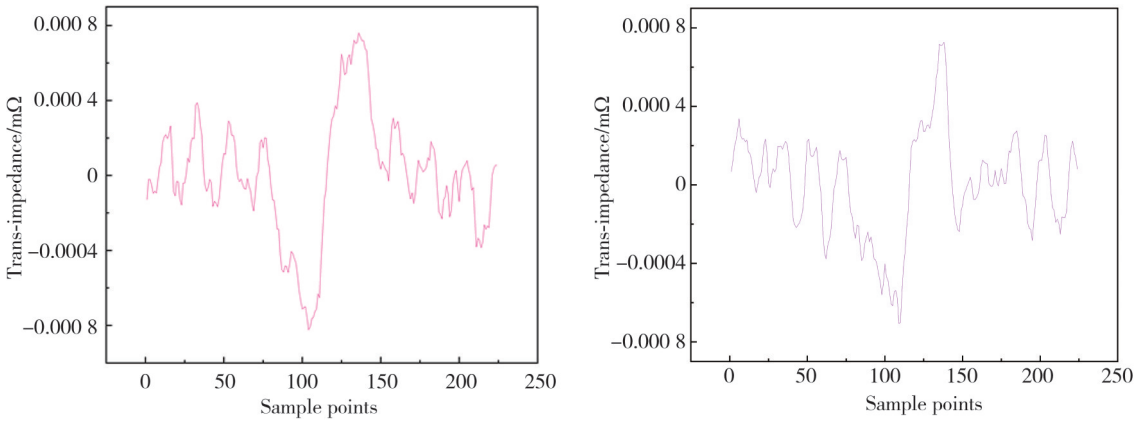

(a) LF at 5.0 mm, real part (b) LF at 6.5 mm, imaginary part

Fig. 14 Output signal corresponding to maximum LF distance of crack detected by a probe at 10 kHz excitation frequency

Fig. 13 depicts the output signals obtained from a linear scan experiment at an excitation frequency of 10 kHz, showing the calculated equivalent impedance values at different LF distances. For the real part of the signal, the characteristic changes from two peaks in a sinusoidal waveform to four peaks. This variation may

be due to changes in the strength and distribution of the eddy current signal, influenced by factors such as the position of the probe relative to the object under test or other environmental conditions.

In order to further determine the evolution of the crack detection performance of the probe at different excitation frequencies with increasing LF, experimentations were conducted at each excitation frequency for crack detection at different LF distances. The output signals are obtained as shown in Fig. 15. Because regardless of the excitation frequency, an increase in the LF distance will result in a decrease in the output signal strength.

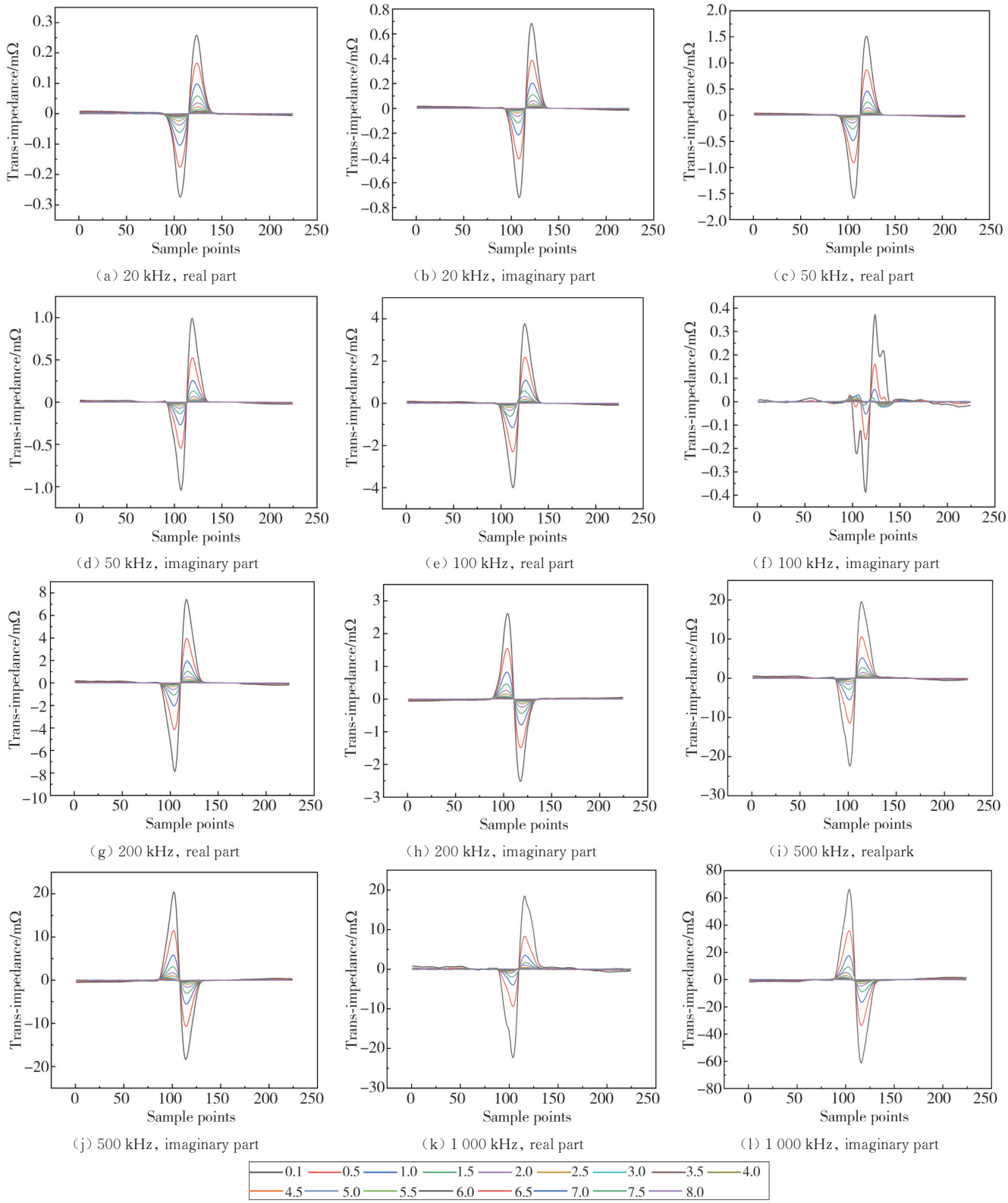

Fig. 15 Signals of different excitation frequencies at different LF distances

Fig.16 shows the variation of the trans-impedance Vpp caused by the change of LF distance at different excitation frequencies. The Vpp decreases exponentially with the increase of the LF distance at the same excitating frequency, which is qualitatively consistent with the FEA results. The Vpp of the real part of the signal trans-impedance at 500 kHz is on average 0.72 mΩ larger than that at 1 000 kHz. Because the excitation current passed into the excitation coil is only 43 mA when the excitation frequency is 1 000 kHz, while the excitating current at 500 kHz is 120 mA, which is 2.8 times larger than that at the excitating frequency of 1 000 kHz. When the excitating frequency is large enough, the excitating current monitored by the multimeter is unstable during the experiment. The excitating current value excluded is not accurate when calculating the trans-impedance. At the same time, due to the interference of factors outside the field during the experiment, such as the installation and positioning error of the probe, the accuracy error of the 3D-scanner and so on, various factors accumulate together to cause the Vpp of the real part of the trans-impedance at 500 kHz to be larger than 1 000 kHz. Table 2 shows the maximum crack LF distance detected by the probe at different excitation frequencies.

Table 2 Maximum LF distance of crack detected by probe

Excitation frequency/kHz	Maximum LF distance/mm	
	Real part	Imaginary part
10	5.0	6.5
20	7.0	6.5
50	8.0	7.5
100	8.0	5.5
200	8.0	8.0
500	6.5	6.5
1 000	4.0	6.5

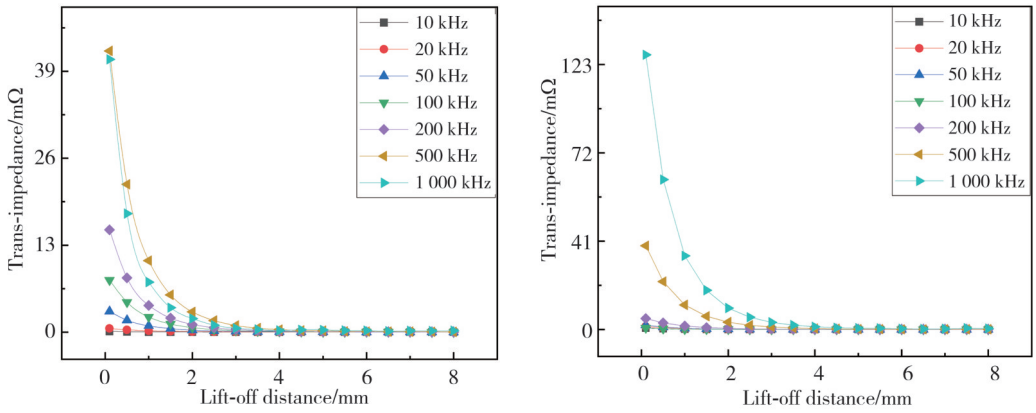

(a) Real part (b) Imaginary part

Fig. 16 Trans-impedance Vpp of probe for different LF distances at different excitation frequencies

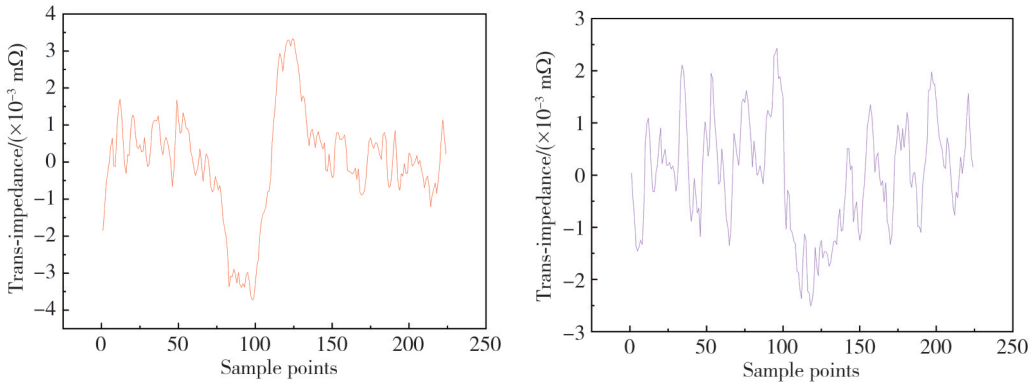

(a) Real part (b) Imaginary part

Fig. 17 Output signal at 200 kHz excitation frequency and 8. 0 mm LF distance

It can be observed that the maximum LF distance of cracks detectable by the two parts of the signal are different at the same excitation frequency. The maximum LF distance of cracks detectable by the probe are also different at different excitation frequencies. At the excitation frequencies of 10 kHz, 20 kHz, 50 kHz, 100 kHz, 200 kHz, 500 kHz, and 1 000 kHz, the maximum LF distance of the real parts of the output signal when a crack can be detected are 5.0 mm, 7.0 mm, 8.0 mm, 8.0 mm, 8.0 mm, 8.0 mm, 6.5 mm, and 4.0 mm, and the imaginary parts are 6.5 mm, 6.5 mm, and 6.5 mm, respectively. The maximum LF distance at 200 kHz is 8.0 mm for the two parts of the signal when cracks can be recognized, compared to the

other excitation frequencies. The maximum LF distance is observed at 200 kHz compared to other excitation frequencies. The output signal at 200 kHz excitation frequency and 8.0 mm LF distance is shown in Fig.17.

4 Conclusions

A single-turn excitation, multi-turn pick-up flexible differential pick-up Koch fractal EC probe was proposed, the equivalent circuit model of the probe was established, and the trans-impedance of the probe was derived. The evolution law of the probe EC on the specimen's surface with the different LF distance was studied by combining simulation and experiment. As well as the LF effect of the probe at each excitation frequency and the influence of the LF distance on the crack detection performance of the probe, the following conclusions were drawn.

1) The equivalent trans-impedance expression of the probe is

$$Z_{\text{req}}=\frac{\omega^2 M_{13}(M_{32\text{L}}-M_{32\text{R}})}{R_3{}^2-\omega^2 L_3{}^2}R_3-\text{j}\frac{\omega^3 M_{13}(M_{32\text{L}}-M_{32\text{R}})}{R_3{}^2-\omega^2 L_3{}^2}L_3.$$

The equivalent trans-impedance is related to ω, M_{13}, $M_{32\text{L}}$, $M_{32\text{R}}$, R_3, and L_3. The variation of the LF distances affects the values of M_{13}, $M_{32\text{L}}$, $M_{32\text{R}}$, R_3, and L_3, which in turn affects the value of the equivalent trans-impedance.

2) The simulation results showed that when the excitation frequency was constant, the similarity between EC distribution shape and excitation coil shape tended to decrease with the increase of LF distance. The EC distribution area was diffused in all directions, gradually evolving into a circle, and the defect intensity was weakened.

3) The experimental revealed that when the excitation frequencies were 10 kHz, 20 kHz, 50 kHz, 100 kHz, 200 kHz, 500 kHz, and 1 000 kHz, the maximum LF distances when cracks could be detected in the real parts of the signal were 5.0 mm, 7.0 mm, 8.0 mm, 8.0 mm, 8.0 mm, 8.0 mm, 6.5 mm, 4.0 mm. And the imaginary parts were 6.5 mm, 6.5 mm, 7.5 mm, 5.5 mm, 8.0 mm, 6.5 mm, 6.5 mm, respectively.

Although this work can achieve crack detection at a LF distance of 8.0 mm, the optimal excitation frequency for the probe to perform large LF crack detection has not yet been determined, so the next step will be to determine the optimal excitation frequency.

Acknowledgements

This work was supported by the National Nature Science Foundation of China (Nos.62471206, 52467002).

Declaration of conflicting interests

The authors have no conflict of interests related to this publication.

References

[1] XIE L, GAO B, TIAN G Y, et al. Coupling pulse eddy current sensor for deeper defects NDT. Sensors and Actuators A: Physical, 2019, 293: 189-199.

[2] TIAN G Y, ZHAO Z X, BAINES R W. The research of inhomogeneity in eddy current sensors. Sensors and Actuators A: Physical, 1998, 69(2): 148-151.

[3] YE C F, ZHANG N, PENG L, et al. Flexible array probe with in-plane differential multichannels for inspection of microdefects on curved surface. IEEE Transactions on Industrial Electronics, 2021, 69(1): 900-910.

[4] ZHANG N, PENG L, HE Y Z, et al. Flexible probe with array tunneling magnetoresistance sensors for curved structure inspection. IEEE Transactions on Instrumentation and Measurement, 2022, 71: 6001109.

[5] ZHANG N, PENG L, TAO X C, et al. Flexible ECT probe with front-end differential setting for inspection of curved CFRP structures. Composites Part B: Engineering, 2021, 227: 109404.

[6] ADEWALE I D, TIAN G, DONG S, et al. Separation of lift-off and defect depth features in magnetic sensor based pulsed eddy current signals. Electromagnetic Nondestructive Evaluation (XVIII). IOS Press, 2015: 211-221.

[7] LI W, CHEN G M, YIN X K, et al. Analysis of the lift-off effect of a U-shaped ACFM system. NDT & E International, 2013, 53: 31-35.

[8] HUANG S L, ZHAO W, ZHANG Y S, et al. Study on the lift-off effect of EMAT. Sensors and Actuators A: Physical, 2009, 153(2): 218-221.

[9] RICCI M, SILIPIGNI G, FERRIGNO L, et al. Evaluation of the lift-off robustness of eddy current imaging techniques. NDT & E International, 2017, 85: 43-52.

[10] TIAN G Y, SOPHIAN A. Reduction of lift-off effects for pulsed eddy current NDT. NDT & E International, 2005, 38(4): 319-324.

[11] YANG B F, LI B, WANG Y J. Reduction of lift-off effect for pulsed eddy current NDT based on sensor design and frequency spectrum analysis. Nondestructive Testing and Evaluation, 2010, 25(1): 77-89.

[12] CHEN K F, GAO B, TIAN G Y, et al. Differential coupling double-layer coil for eddy current testing with high lift-off. IEEE Sensors Journal, 2021, 21(16): 18146-18155.

[13] HOSHIKAWA H, KOYAMA K, KARASAWA H. A new ECT surface probe without lift-off noise and with

phase information on flaw depth. Review of Progress in Quantitative Nondestructive Evaluation, 2001, 20: 969-976.
[14] HUANG H, TAKAGI T. Crack shape reconstruction from noisy signals in ECT of steam generator tube//2000 26th Annual Conference of the IEEE Industrial Electronics Society. IECON2000. 2000 IEEE International Conference on Industrial Electronics, Control and Instrumentation. October 22-28, 2000, Nagoya, Japan. New York: IEEE, 2000: 2507-2512.
[15] SHU L, SONGLING H, WEI Z, et al. Improved immunity to lift-off effect in pulsed eddy current testing with two-stage differential probes. Russian Journal of Nondestructive Testing, 2008, 44(2): 138-144.
[16] CHEN G L. Two novel information entropy indices for analysis of the eddy current distribution. Entropy, 2018, 20(9): 699.
[17] CHEN G L, CAO Z. Quantitative evaluation of eddy current distribution by relative entropy and cross entropy. Measurement and Control, 2021, 54(3/4): 164-169.
[18] CHEN G L, ZHANG W M, PANG W H. Koch curve fractal geometry excitation probe for eddy current non-destructive testing. Measurement, 2018, 124: 470-478.
[19] CHEN G L, SONG Z B, JIN W Y. A novel planar differential excitation eddy current probe based on the fractal Koch curve. Measurement, 2022, 193: 110947.
[20] CHEN G L, LI Z F, CAO Z, et al. A differential excitation eddy current probe based on the novel annular fractal curve for defects inspection. IEEE Sensors Journal, 2022, 22(16): 15903-15915.

柔性差测量科赫分形涡流传感器提离效应分析

陈国龙*, 樊　乐, 张帅帅, 韩　瑜, 李奕欣, 张雁龙

兰州理工大学 机电工程学院, 甘肃 兰州 730050

摘　要: 本研究采用有限元仿真和实验方法, 探究了柔性差测量分形科赫涡流传感器在不同激励频率下随着提离距离增加对裂纹检测性能的演化规律, 以及传感器在可检测到裂纹时的最大提离距离。随着提离距离的增加, 感应涡流的分布形状发生变化, 导致激励线圈形状的相似性降低, 感应涡流的分布范围扩展, 最终导致输出信号的强度减弱。实验结果显示, 当激励频率分别为10 kHz、20 kHz、50 kHz、100 kHz、200 kHz、500 kHz和1 000 kHz时, 传感器输出信号的实部在检测到裂纹时的最大提离距离分别为5.0 mm、7.0 mm、8.0 mm、8.0 mm、8.0 mm、6.5 mm和4.0 mm; 虚部则分别为6.5 mm、6.5 mm、7.5 mm、5.5 mm、8.0 mm、6.5 mm和6.5 mm。

关键词: 涡流检测; 提离效应; 无损检测; 裂纹检测; 分形几何

引用格式: CHEN Guolong, FAN Le, ZHANG Shuaishuai, et al. The lift-off effect analysis of flexible differential pick-up koch fractal eddy current probe. Journal of Measurement Science and Instrumentation, 2024, 15(4): 432-444.